Project information

Project full title	Connecting Russian and European Measures for Large-scale Research Infrastructures – plus
Project acronym	CREMLINplus
Grant agreement no.	871072
Instrument	Research and Innovation Action (RIA)
Duration	01/02/2020 – 31/01/2024
Website	www.cremlinplus.eu

Deliverable information

Deliverable no.	D5.2 (D45)
Deliverable title	Status report on R&D work on inner tracker for the SCT detector
Deliverable responsible	INFN
Related Work-Package/Task	WP5; Task 5.4
Type (e.g. Report; other)	Report
Author(s)	
Dissemination level	Public
Document Version	
Date	
Download page	https://www.cremlinplus.eu/results/deliverables/

Document information

Version no.	Date	Author(s)	Comment
1.1	10.01.2022	Giovanni Bencivenni, Lev Shekhtman, Gianfranco Morello, Erika De Lucia, Lia Lavezzi	

This project has received funding from the European Union's Horizon 2020 research and innovation programme under grant agreement No. 871072.

Table of Contents

Development and design of an Inner Tracker for the SCT detector

The aim of this task is the development of an inner tracker (IT) for the SCTF detector (SCTD). Two different IT concepts are going to be developed and tested: a compact TPC with MPGD readout under BINP responsibility and a cylindrical μ-RWELL (C-RWELL) chamber designed and built by the INFN-Ferrara and LNF collaboration.

1. Compact Time Projection Chamber as IT for the SCTF detector

A compact Time Projection Chamber (TPC) can provide several advantages as Inner Tracker of the SCTD. The Inner wall of the TPC can be made very thin and, thus, it can provide the lowest momentum threshold of soft hadrons that can be detected in the sensitive volume. The number of clusters on track in the TPC volume can reach several hundred that will allow very high momentum resolution for soft tracks that do not leave the TPC volume. Energy deposition per track will allow to distinguish between soft hadrons and electrons in the presence of intense background.

As the Inner tracker has to work very close to the interaction point and is surrounded by the final focus magnetic system, the main issue that has to be addressed by the R&D program, is study of the background flux and its influence on the TPC operation. Thus, the R&D includes several directions of the simulations studies, such as: simulation of the background flux in the

This project has received funding from the European Union's Horizon 2020 research and innovation programme under grant agreement No. 871072.

SCTD and in the Inner Tracker region in particular; simulation of electron transport in the TPC volume and in the readout detector for different gas mixtures and selection of the best mixtures; simulation of the ion space charge effects based on the results of the background simulations.

Another part of the R&D program is development of the TPC prototype. Main objectives of this work are the following: measurement of spatial resolution (on tracks) as a function of readout pad size, gas mixture, reconstruction algorithm, readout electronics and its parameters (clock frequency, shaping time, amplification, noise), track angle, and validation of simulation; analysis and solving of all technological issues during construction; comparison of several detector technologies for the readout detector (GEM, µ-RWELL+GEM, thick-RWELL+GEM); assessment of existing ASICs for TPC readout (DMXG64, VMM3a…) and input for the development of specialized ASIC.

1.1. Simulation of background flux

Simulation of the background flux is performed with the FLUKA package [1,2]. Primary background is generated by two processes: two-photon interaction $e^+e^- \rightarrow \gamma^*\gamma^* \rightarrow e^+e^-e^+e^-$ ($E_{e^+e^-} > 2$ MeV), total cross-section is 2.9 mbarn at 3 GeV per beam, generator DIAG36 [3]; radiative Bhabha $e^+e^- \rightarrow e^+e^-\gamma(n\gamma)$ ($\theta > 5$ mrad, $E_\gamma > 1$ MeV), total cross-section is 1.2 mbarn at 3 GeV per beam, generator BHWIDE [4]. Part of the detector model around the interaction point, including the TPC region is shown in Figure 1. All critical dimensions are shown in the figure. The maps of charged particle fluxes for the Inner Tracker region, obtained by simulations, are shown in Figure 2. At the inner radius of the TPC, 3 cm, the average particle flux along Z is about 10^5 particles per second per cm^2. It quickly falls with a radius reaching 1000 particles per second per cm^2 at 10 cm. However, the background particle flux is not uniform along Z. As the electron drift velocity for the most popular gas mixtures such as $Ar + 25\%CO_2$ is about 5 cm/µs at a moderate drift field of 1000 V/cm that makes electron drift time of about 6 µs, we consider next maps of background particles tracks for this accumulation time. Figure 3 shows the R-Z map of energy depositions accumulated in the TPC volume in 6 µs. It is evident that most of the background particles have very low momentum, and many tracks have their origin not in the interaction point but in the flanges and the first cones of the final focus system.

Number of charged particle tracks crossing the TPC volume as a function of Z coordinate is shown in Figure 4 for the first flanges and cones made of steel (Figure 4 left) and of titanium (Figure 4 right). Change of material from steel to titanium helps to reduce the background flux by a factor of ~20%

This project has received funding from the European Union's Horizon 2020 research and innovation programme under grant agreement No. 871072.

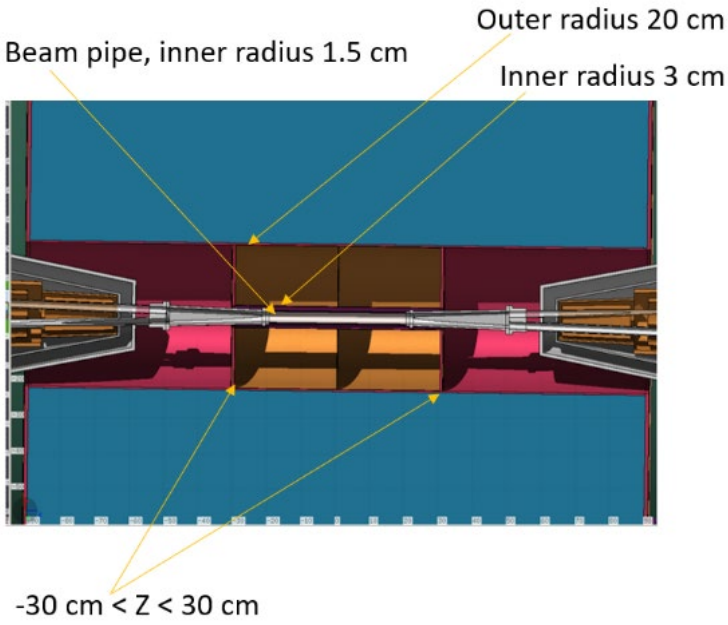

Figure 1. Part of the detector geometry around the interaction point, including TPC and parts of the final focus magnets.

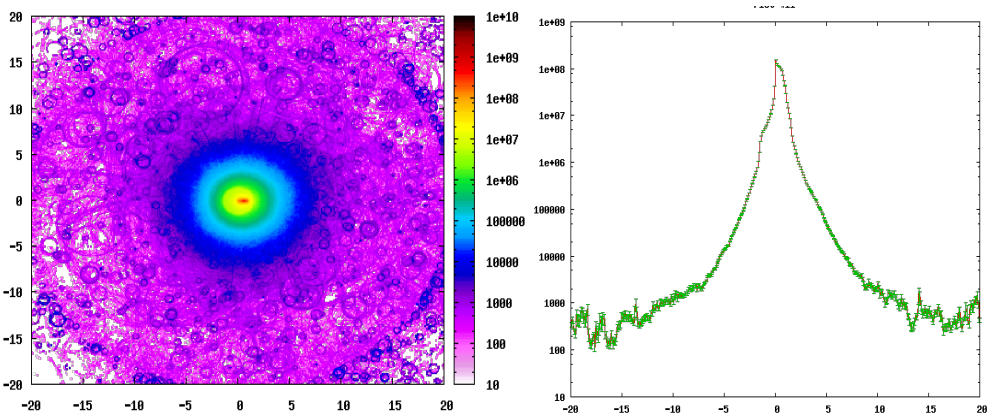

Figure 2. X-Y map of charged particle flux in the IT region: (left) X-Y map averaged in $|Z| < 30$ cm, X and Y scales are in cm, colour scale is in particles per second per cm^2; (right) cross-section of the X-Y map at $|Y| < 1$ cm, X map is in cm, Y map is in particles per second per cm^2.

This project has received funding from the European Union's Horizon 2020 research and innovation programme under grant agreement No. 871072.

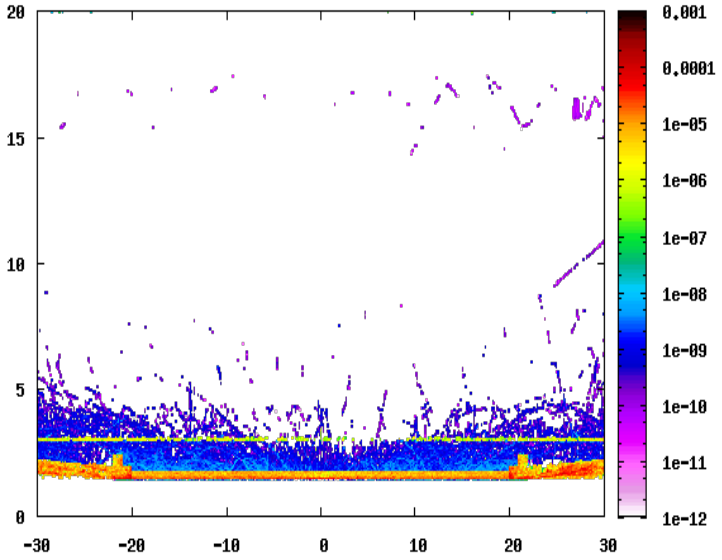

Figure 3. R-Z map of energy depositions accumulated in the TPC volume in 6 μs.

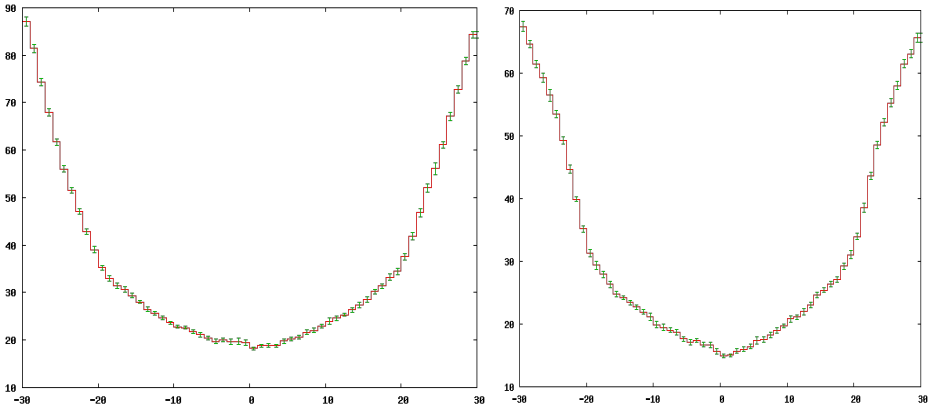

Figure 4. Number of tracks crossing the TPC volume as a function of the Z-coordinate for steel flanges and cones (left) and for titanium flanges and cones (right). Horizontal scale is in cm, the vertical scale is in number of tracks per TPC acceptance.

1.2. Simulation of electron transport in TPC and choice of the gas mixture

In order to determine an optimal gas mixture for the best spatial resolution, short electron drift time at a comfortable high voltage applied to the TPC field cage, special simulations, based on GARFIELD++ code, are performed. Tracks of 1 GeV electrons directed along the Z-axis were drifting in the TPC field and were transported through a four-GEM cascade. Simulation of the avalanches in GEMs was performed and corresponding extra diffusion of electron clusters was determined. Spatial resolution was determined for pieces of tracks that correspond to 50 ns of drift time. For each such piece the transverse diffusion was applied, and charges were distributed over readout pads. Then the center of gravity (COG) method was applied to determine the final coordinate of each piece of track, and the distribution of residuals between actual positions and simulated positions was obtained. Spatial resolution was determined as rms of such distribution. The results of these simulations for three gas mixtures are shown in Figure 5.

This project has received funding from the European Union's Horizon 2020 research and innovation programme under grant agreement No. 871072.

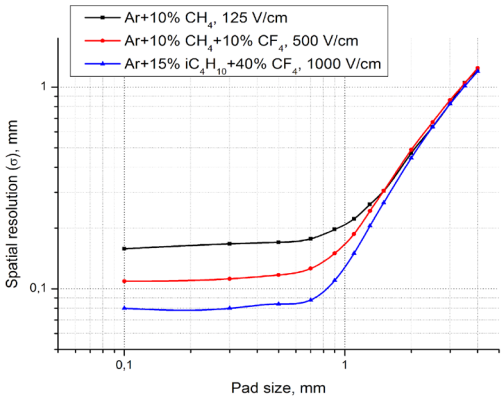

Figure 5. Spatial resolution as a function of readout pad size for three gas mixtures: $Ar + 10\%CH_4$ at 125 V/cm drift field; $Ar + 10\%iC_4H_{10} + 10\%CF_4$ at 500 V/cm; $Ar + 15\%iC_4H_{10} + 40\%CF_4$ at 1000 V/cm.

These three mixtures are chosen for the following reasons: $Ar + 10\%CH_4$ provides fast drift at the lowest field, drift velocity is 6 cm/μs at 125 V/cm; $Ar + 10\%iC_4H_{10} + 10\%CF_4$ is the fastest at moderate field of 500 V/cm; $Ar + 15\%iC_4H_{10} + 40\%CF_4$ provides the best spatial resolution, however, at rather high drift field of 1000 V/cm. From Figure 5 we can see that the best spatial resolution is reached for all mixtures at the pad size below 0.7 mm. The best resolution of 80 μm can be obtained for $Ar + 15\%iC_4H_{10} + 40\%CF_4$.

1.3. Simulation of ion space charge effects

Ion space charge in the TPC field cage can significantly distort electric field map and that will result in systematic distortion of track positions. In order to estimate such distortion a dedicated simulation was performed. Ion space charge distribution along radius was calculated according to the background charged particles flux distribution (see Figure 2). Distribution of space charge along Z was uniform. For the calculation of actual space charge density, the gas amplification of the readout detector was fixed at 10000 and ion back-flow (IBF) value was varied from 1% to 5%. We assumed that we would be able to optimize the readout detector in order to reach the necessary IBF value at a gain of 10000. After the actual space charge distribution in the TPC volume is fixed, the electric field is calculated with the COMSOL program. Then the deviation of electron drift passes from the straight lines were calculated. An example of the map of electron drift lines deviations for $Ar + 15\%iC_4H_{10} + 40\%CF_4$ mixture at initial drift field of 1000 V/cm, and IBF equal to 1% is shown in Figure 6.

This project has received funding from the European Union's Horizon 2020 research and innovation programme under grant agreement No. 871072.

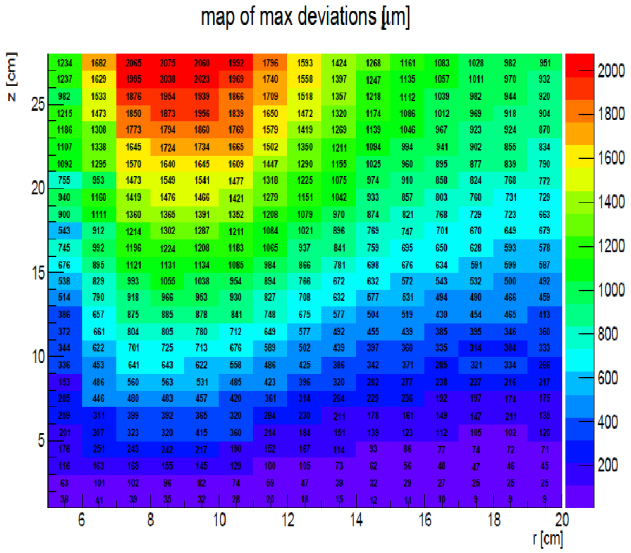

Figure 6. Map of the electrons drift lines deviations for the gas mixture Ar+15%iC4H10+40%CF4 at 1000 V/cm initial drift field, gas gain of the readout detector of 10000 and IBF=1%.

The results obtained for different gas mixtures and IBF values are summarized in Table 1.

Table 1. Summary of the results of the simulations of space charge effects in the TPC.

Gas mixture	E, V/cm	dn_e/dx, cm^{-1}	t_{drift}, s	IBF	Max deviation, mm
$Ar + 10\%CH_4$	125	90	0.14	1%	94
$Ar + 10\%CH_4 + 10\%CF_4$	500	90	0.03	1%	5.0
$Ar + 10\%CH_4 + 10\%CF_4$	500	90	0.03	3%	15.1
$Ar + 15\%iC_4H_{10} + 40\%CF_4$	1000	112	0.02	1%	2.1
$Ar + 15\%iC_4H_{10} + 40\%CF_4$	1000	112	0.02	3%	6.2

From the table we can see that for Ar+10%CH_4 mixture the maximum deviation of electrons drift line reaches 94 mm. This very large deviation occurs due to low drift field and, thus, very high ion charge density. Ion drift time for this mixture is only 0.14 s. It is clear that this mixture cannot be applied in spite it is very attractive due to rather high electron drift velocity at low field. Other two gas mixtures show moderate deviations of electrons drift lines even at IBF value of 3%.

This project has received funding from the European Union's Horizon 2020 research and innovation programme under grant agreement No. 871072.

1.4. The TPC prototype

The TPC prototype consists of two main parts: the field cage with high voltage distribution, resistive divider, high voltage flange and electrode, and the readout flange with the detector. The present TPC prototype has only the outer cylinder wall and no central pipe. The outer wall of the field cage is made of four printed circuit boards 0.5 mm thick, shown in Figure 7 with their photo before mounting.

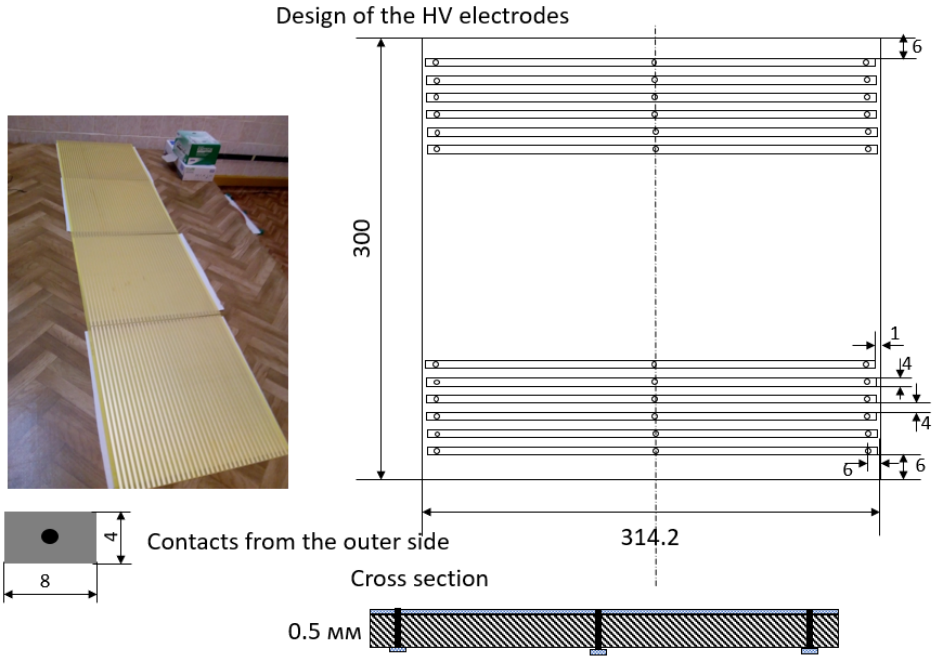

Figure 7. Design and photograph of the panels for the side wall of the TPC field cage.

These four plates were glued together and then bent and glued to form the cylinder. The ends of the cylinder were reinforced with glass fiber rings, and the high voltage electrode was glued to the reinforcement ring from the high voltage side (Figure 8). From the readout side a special aluminum ring with a gasket was glued to the reinforcement ring in order to attach the readout detector. Schematic view of this part with drawings of the fixation ring are shown in Figure 9. The field cage with glued fixation ring and mounted resistive divider is shown in Figure 10. The fixation ring will keep the readout flange that will consist of three parts, shown in Figure 11: the readout flange reinforcement ring, the readout flange wall and the reinforcement square. The readout flange will keep on it a special aluminum insert that will place the readout detector at a certain distance from the zero potential plane of the field cage in order to align the potential of the top electrode of the readout detector with potential at the side wall of the field cage. The insert will be glued on two pairs of parts, shown in Figure 12. On top of the insert the readout PCB will be attached that will keep a stack of three or four GEMs as a first variant of the amplifying structure. In future we are going to try a combination of GEMs with muRWELL or thick RWELL. Design of the readout PCB is shown in Figure 13. It contains 25 4x4 mm^2 pads positioned at a pitch of 5 mm and will allow connecting front-end amplifiers for the first tests. In future we are going to design the readout PCB with smaller pads, down to 0.5 mm that will be connected to the readout electronics

This project has received funding from the European Union's Horizon 2020 research and innovation programme under grant agreement No. 871072.

based on ASICs through connectors at the back side. All parts have been ordered and expected to be delivered within February 2022.

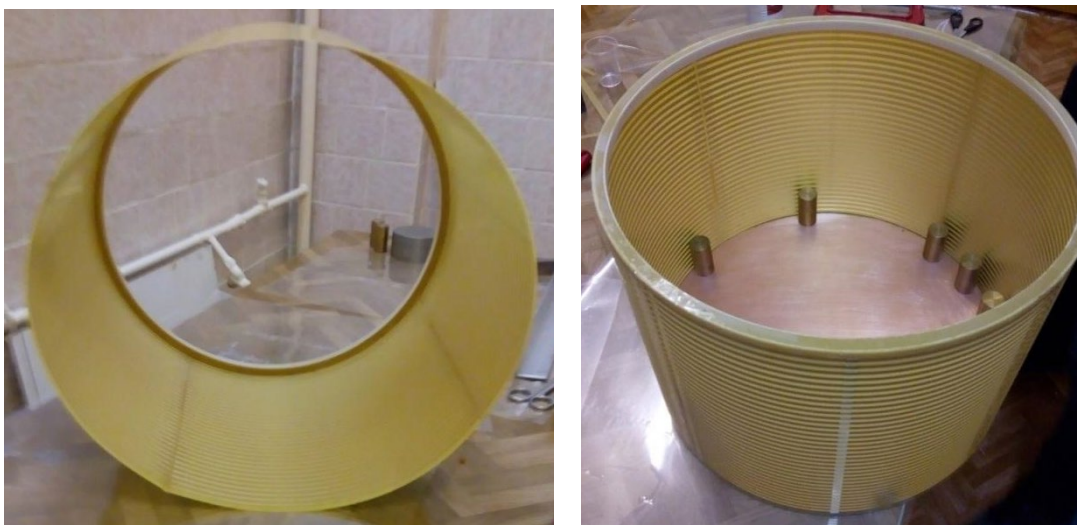

Figure 8. The cylinder with HV distribution strips is glued with glass fiber reinforcement from the HV side (left); gluing of the HV electrode to the inner side of the reinforcement ring (right).

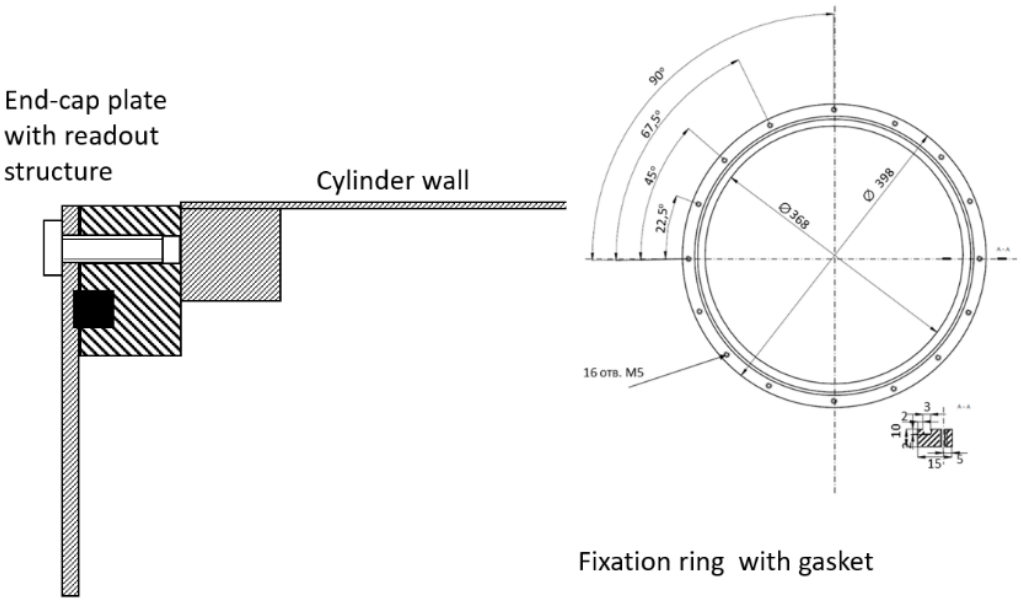

Figure 9. Schematic view of the readout side and design drawing of the fixation ring for the readout detector.

This project has received funding from the European Union's Horizon 2020 research and innovation programme under grant agreement No. 871072.

Figure 10. Assembled field cage with the fixation ring glued and resistive divider mounted.

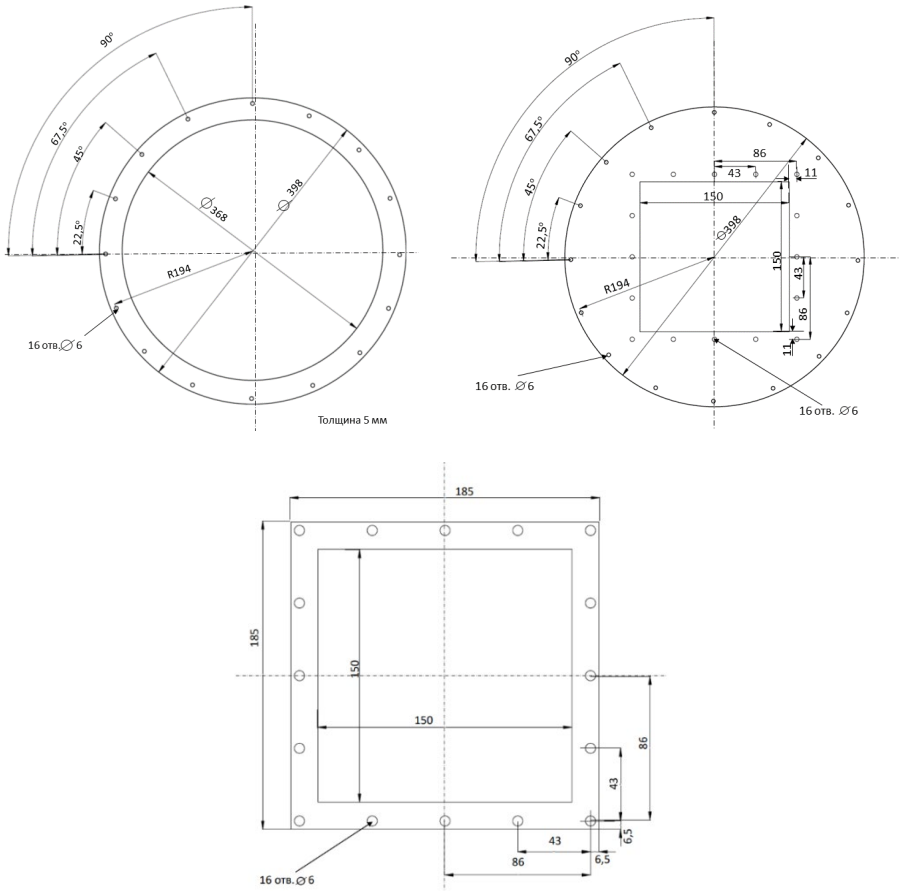

Figure 11. Drawings of the parts of the readout flange: (left) reinforcement ring; (right) flange wall; (bottom) reinforcement square.

This project has received funding from the European Union's Horizon 2020 research and innovation programme under grant agreement No. 871072.

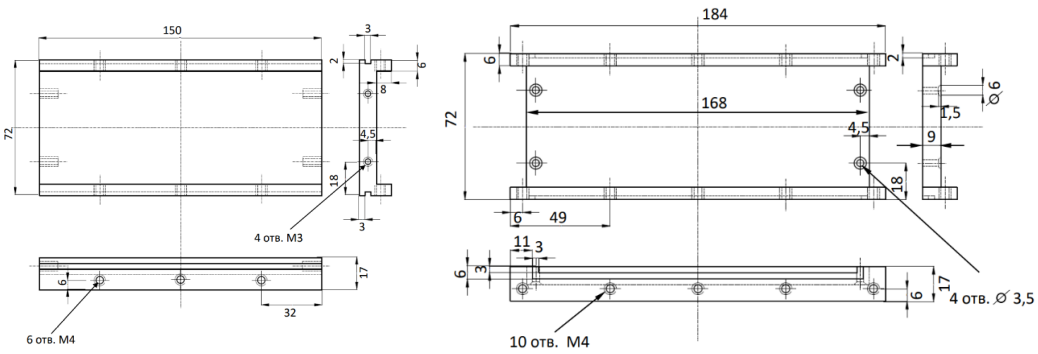

Figure 12. Drawings of the parts of the insert.

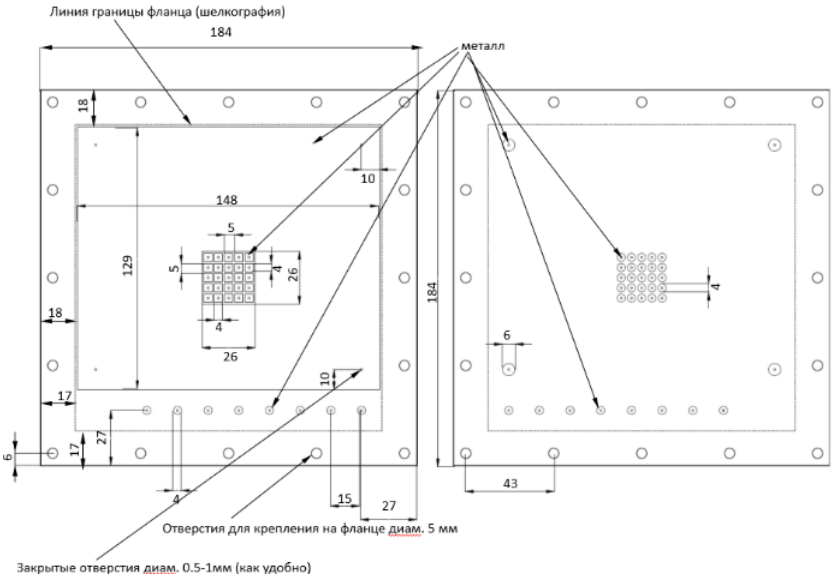

Figure 13. Design of the first version of the readout PCB.

2. Low-mass modular cylindrical-RWELL as IT for the SCTF detector

The cylindrical-RWELL (C-RWELL) is a low material budget $\mathcal{O}(1\%)X_0$ full cylindrical IT based on the μ-RWELL technology. The μ-RWELL [6,7] is a resistive MPGD composed of two PCBs: a mono-layer PCB acting as the cathode, defining the gas detector gap, and a μ-RWELL_PCB that couples in a unique structure the electron amplification (a well-patterned GEM-like matrix) and the readout stages, as shown in Figure 14. A 50 μm thick polyimide foil, copper clad on the top side and sputtered with Diamond Like Carbon (DLC, [8]) on the opposite (bottom) side, is coupled to a standard PCB readout board, through a 50 μm thick pre-preg foil. The thickness of the DLC layer (typically in the range 10÷100 nm) is adjusted according to the desired surface resistivity value (10 ÷100 MΩ/square) in order to provide discharge suppression as well as current evacuation. A chemical etching process of the polyimide foil is performed on the top surface of the overall structure in order to create the WELL pattern: truncated cone wells of 70 μm (50 μm) top (bottom) in diameter and 140 μm pitch) that constitutes the amplification stage. The high voltage applied between the copper and the resistive DLC layers produces the required electric field within the WELLs that is necessary to develop charge amplification, Figure 15. The signal is capacitively collected at

This project has received funding from the European Union's Horizon 2020 research and innovation programme under grant agreement No. 871072.

the strips/pads on the readout board. The introduction of the resistive layer allows to achieve large gains ($\varepsilon 10^4$) with a single amplification stage, while partially reducing the capability to stand high particle fluxes.

The C-RWELL is mainly based on the flexibility of the base material used for the manufacturing of its amplification/readout stage. In addition, being designed as an "openable" and "modular" detector it will be a highly reliable and performing IT, while the spark suppression mechanism, intrinsic to the μ-RWELL technology, makes the operation of this detector more safe with respect to other MPGD based devices.

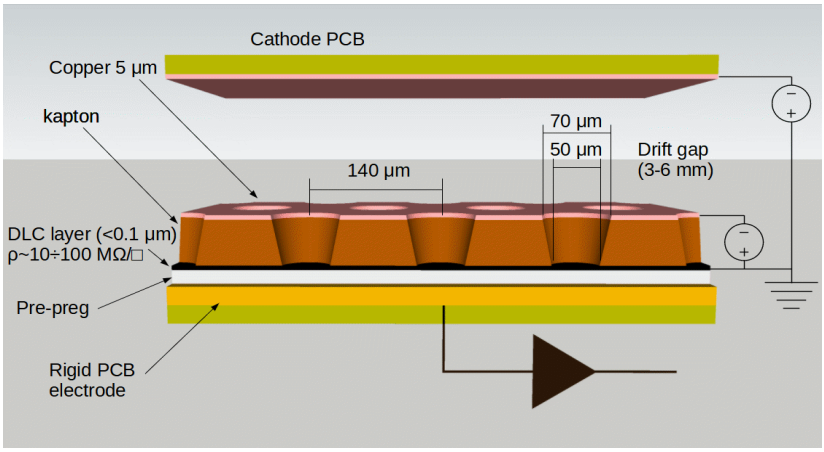

Figure 14. Basic layout of a μ-RWELL

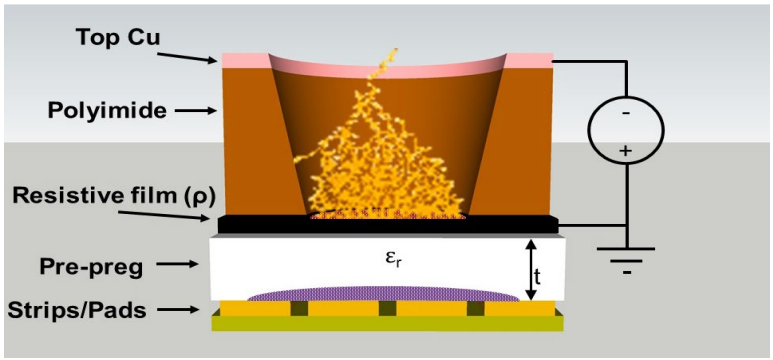

Figure 15. Principle of operation of the μ-RWELL.

The reconstruction of the particle track traversing the gas sensitive gaps will be based on a combination of two algorithms: Charge Centroid (CC) and μ-TPC. Tests performed with planar prototypes show that an almost uniform space resolution below 100 μm over a wide angular range of track incidence (0 ÷ 45°) is obtained [9]. As shown in Figure 16, at low drift fields the measured space resolution improves reaching values down to 65 μm.

This project has received funding from the European Union's Horizon 2020 research and innovation programme under grant agreement No. 871072.

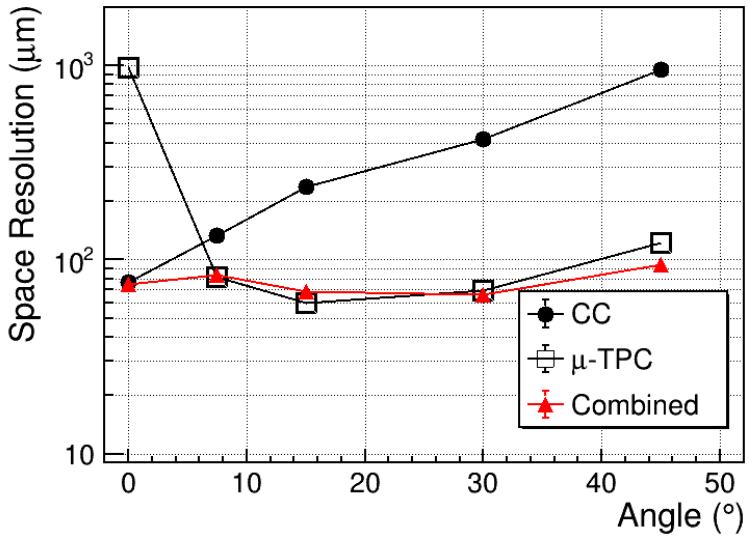

Figure 16. Comparison of the two algorithms with their combined reconstruction, at a drift field $E_D = 1$ kV/cm.

2.1. Design and construction of the C-RWELL prototype

The main feature of the μ-RWELL is to have the amplification stage, the resistive layer and the readout board embedded in one single element. The possibility to realize this element with flexible substrates makes the technology suitable for non-planar geometry. Two ideas of C-RWELL are under study, both based on a common double-faced cathode layout. In one case (Figure 17 left) a two large radial gaps option for a 10 cm global sampling gas along the radial direction has been considered, while in the second case (Figure 17 right) four thinner gaps for a 4 cm global sampling gas are foreseen. Depending on the material choice, the former layout could be realized with a global material budget in the range 0.75 ÷ 0.86% X_0, while the latter layout in the range 1.46 ÷ 1.72% X_0. For both layouts, the cylindrical μ-RWELL_PCB is divided in three "roof tiles" detectors that, thanks to the possibility to open (and re-close) the cylindrical support, are removable in order to be replaced in case of malfunctioning.

A 1 cm large mono-gap prototype, composed of coaxial cylindrical anode and cathode structures, has been designed (Figure 18) and realized by LOSON S.r.l., a company with a remarkable expertise in composite elements. The substrate for the electrodes is Millifoam. The dimensions and all relevant numbers of the prototype are summarized in Table 2.

This project has received funding from the European Union's Horizon 2020 research and innovation programme under grant agreement No. 871072.

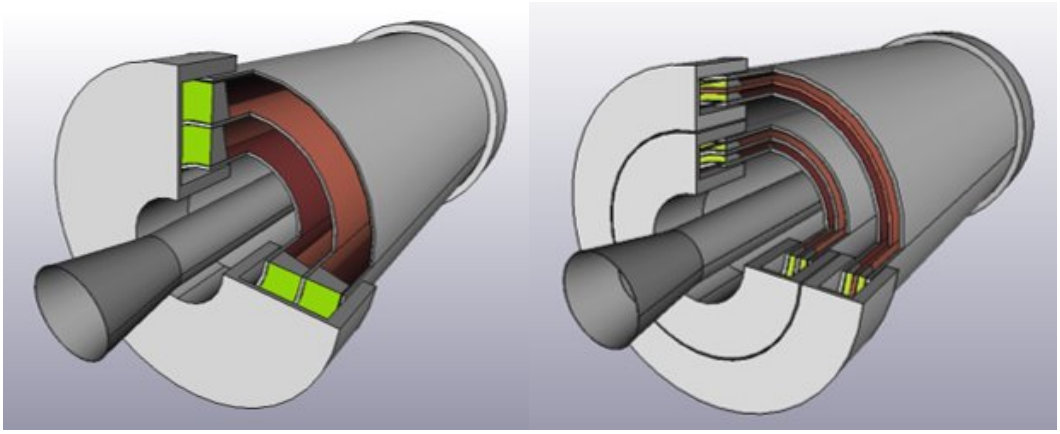

Figure 17. The two options for the Inner Tracker: on the left the double large gas gap; on the right a pair of double thinner gas gaps.

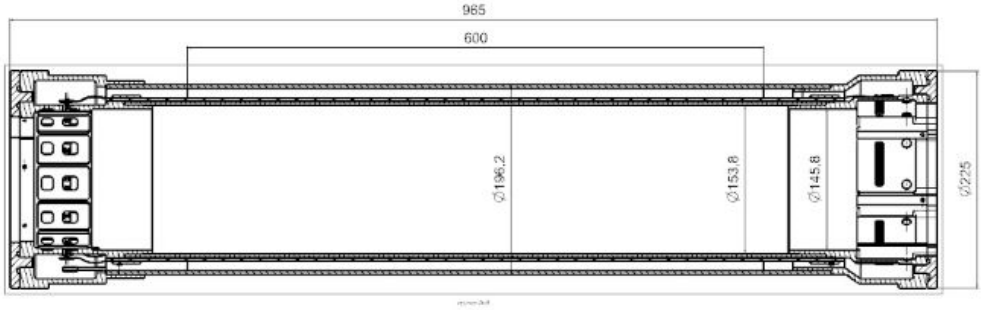

Figure 18. Cross-section of the C-RWELL mono-gap prototype.

Table 2. Dimensions (mm) and relevant numbers of the C-RWELL prototype

anode dia.	cathode dia.	drift size	active length	# HV chs	# r/out chs	strip pitch
168.5	188.5	10	600	12	768	0.68

2.1.1. The cathode

The cathode is the outermost electrode of this prototype, it has been stratified starting from the kapton-copper foil (Figure 19 left). The stratification has been continued with a skin of fiberglass (Figure 19 right), a layer of Millifoam (Figure 20), a second fiberglass skin and a copper layer operating as a Faraday cage. The flanges at the two edges of the cathode are made of Peek (standing for polyether ether ketone).

This project has received funding from the European Union's Horizon 2020 research and innovation programme under grant agreement No. 871072.

Figure 19. Cathode lamination: the initial copper layer (left) and the fiberglass deposition (right).

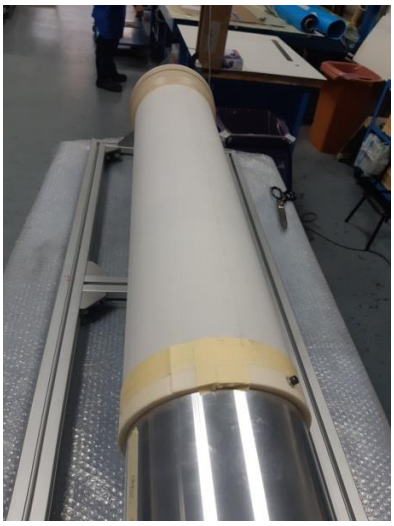

Figure 20. Millifoam layer glued on cathode.

2.1.2. The anode

The cylindrical anode is composed of three roof-tiles, each then with a radial coverage of 120° (Figure 21). Each flexible μ-RWELL_PCB and built at the CERN-PH-DT Workshop (Figure 22), is equipped with axial strips, parallel to the axis of the cylinder. The roof-tile support for the μ-RWELL_PCB is done with a 3 mm thick Millifoam (Figure 23): this material must be handled very carefully, so it has been quite challenging to obtain a certified procedure to realize such light roof tile at the same time robust enough to keep the μ-RWELL_PCB at a given shape with a very tight mechanical tolerance (100 um) on the radial direction.

The anode flanges, realized in Peek, have been designed with proper windows to host the boards for the HV distribution (Figure 24 left) and the interface boards for the connection of front-end electronics (Figure 24 right).

The presence of these openings required a dedicated test for the gas tightness of the flange-boards system. The boards are actually glued on the inner surface of the flange with Araldite 2011. The gas tightness test has been performed with a dedicated tool (Figure 25), where the system has been flushed with nitrogen, comparing the entering and the exiting flow; a second test has been done setting a 20-mbar over-pressure (condition much worse than the operating

This project has received funding from the European Union's Horizon 2020 research and innovation programme under grant agreement No. 871072.

condition, that foresee <5 mbar gas over-pressure) inside the flange and monitoring the pressure drop as a function of the time. The over-pressure decreased by about 1 mbar after 2 hours, when the test was stopped and considered successful. The construction of the prototype was completed in December 2021 (Figure 26) and the final assembly of the whole detector, including the flexible detector tiles, will be performed in the next few months.

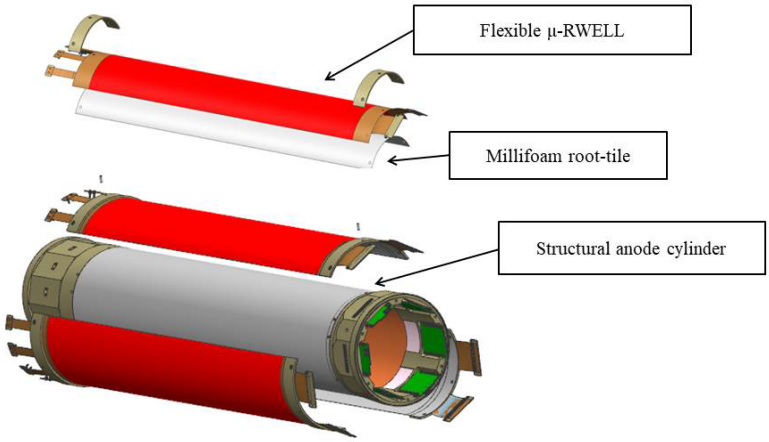

Figure 21. Sketch of the assembly of the three roof-tile detectors on the anode cylinder. The anode cylinder is made of composite material: FR4 - Millifoam - FR4 sandwich plus an additional finely machined layer of Millifoam.

Figure 22. Flexible μ-RWELL_PCB detector tiles manufactured at the CERN-PH-DT Workshop.

Figure 23. Millifoam support for the tile.

This project has received funding from the European Union's Horizon 2020 research and innovation programme under grant agreement No. 871072.

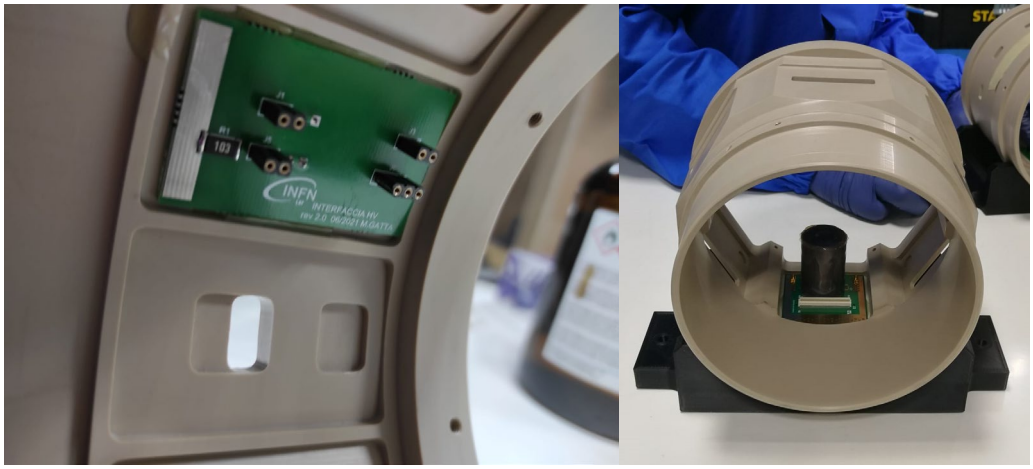

Figure 24. A HV distribution board glued on the flange (left) and a FEE intermediate board glued on the opposite flange (right).

Figure 25. Setup for the gas tightness tests of the HV flange (left) and FEE flange (right).

This project has received funding from the European Union's Horizon 2020 research and innovation programme under grant agreement No. 871072.

Figure 26. Assembly of the prototype. From top left: the cathode mounted on the assembly machine; the rectified Millifoam support for the detector tiles; the insertion of the cathode on the cylindrical anode.

2.2. Detector Simulation

The software framework Aurora, based on Gaudi, is a key element of the SCTD project. The implemented strategy for the C-RWELL software tools starts with the geometry description, using DD4HEP and included in Aurora version 1.0.1, the simulation of energy deposition and detector response, and the digitization stage ready to be merged in the official software. For the detector response parameterization, a fast simulation has been developed starting from a dedicated simulation software used for BESIII triple-GEM detectors [10] and adapting it to the μ-RWELL detector with the aim of simulating the resistive stage and validating it with DATA/MC matching of known planar detector configuration studied at test beams. To this extent during October 2021 a test beam was performed at CERN H8 area with planar μ-RWELL realized with different values of resistivity.

The software strategy and implementation will be described together with preliminary results obtained with the C-RWELL detector simulation in the SCT Aurora framework and the dedicated detector response parametrization.

This project has received funding from the European Union's Horizon 2020 research and innovation programme under grant agreement No. 871072.

2.2.1. Geometry description

For the time being the geometry of the second option for the C-RWELL detector (see Figure 17 right) has been inserted in the official simulation DD4HEP framework. In this case four small gaps with 4 cm global sampling gas are foreseen. As for the materials and cathode and anode details, the mechanical drawings and description have been used. The new materials characterizing the detector have been inserted in the sub-detectors material listing: FR4, DLC and so far honeycomb. Detector sensitive layers and materials have been defined to allow hits generation to be performed.

Figure 27 shows the first results from the full detector simulation: on the left the 3D distribution of Geant4 hits generated and saved in the C-RWELL detector with

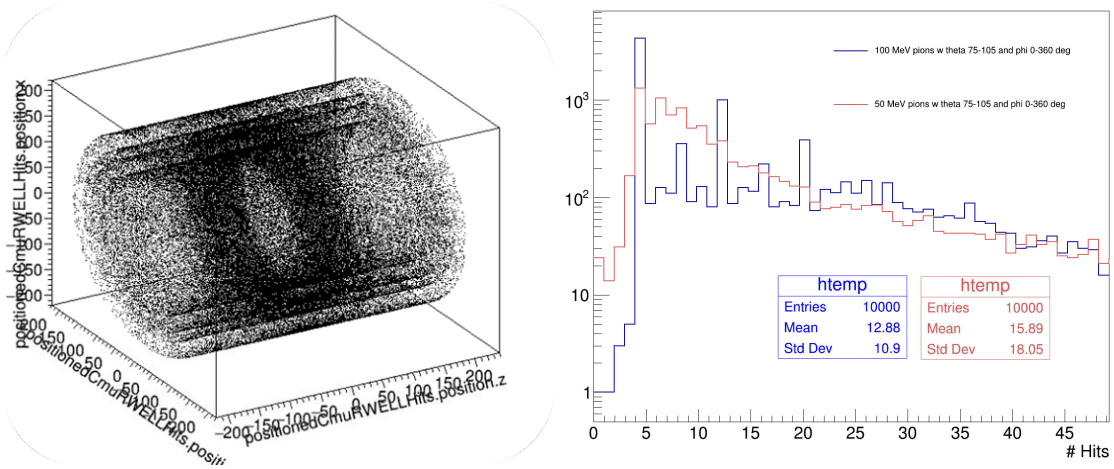

Figure 27. Full detector simulation: 3D distribution of hits in C-RWELL from 100 MeV pions (left) and the number of hits in C-RWELL obtained with 50 MeV pions in red and 100 MeV pions in blue (right).

100 MeV pions from ParticleGun with 75 < theta < 105 degrees and 0 < phi < 360 degrees. Figure 27 right shows the comparison between the distribution of the number of hits in the C-RWELL detector obtained with 50 MeV pions in red and with 100 MeV pions in blue respectively. This is part of the soft pion study aiming at the evaluation of the vertex reconstruction efficiency and resolution for pions with momentum p < 100 MeV.

2.2.2. Digitization

The complete simulation of the C-RWELL includes also the response of the detector to the energy deposition, with the description of the formation of the electronic signal inside the detector. The output of the digitisation is the raw hit, which has the same characteristics of the hit produced by the real detector, which in the case of the C-RWELL consists in the charge and time measurements associated with the fired strip. From this raw information the position where the particle passed inside the detector volume can be reconstructed and used in track finding and track fitting algorithms.

The response of the detector can be modeled with different levels of approximation.

A C-RWELL digitization package has been implemented in the Aurora framework and is ready to be uploaded in the project common git repository. Currently it hosts a simplified

This project has received funding from the European Union's Horizon 2020 research and innovation programme under grant agreement No. 871072.

digitization procedure, which skips the full description of the physics inside the detector and simply transforms the Monte Carlo (MC) point from Geant4 directly into a reconstructed hit. The reconstructed hit contains the information on the position, which is computed at the center of the drift gap, starting from the MC entrance and exit points obtained by Geant4, with an additional smearing which accounts for the expected position resolution (see Figure 28). Additionally, the reconstructed hit provides the measured charge, computed starting from the total energy deposit from the MC, and the signal time, calculated as the average value of the time associated to each MC point.

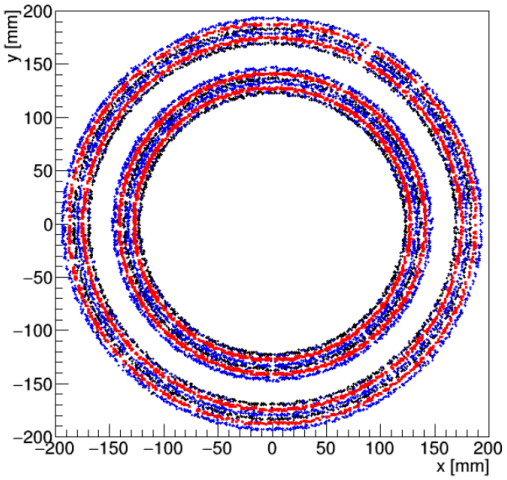

Figure 28. Transverse view of the MC entrance (black) and exit (blue) points in the gas gaps. The digitized hits are drawn in red color and are at the center of the gas gap. One thousand positive pions with momentum 200 MeV/c were simulated.

2.2.3. Detector Response Parametrization

The full digitization is under development in a standalone code. It takes into account the various physics processes that play a role in the raw hit formation. It is composed of several steps, one for each independent physics effect.

The production of primary and secondary ionization in the gas gap is simulated following Poisson statistics, the detector gain is reproduced by sampling from the Polya distribution, the effect of the material (and possibly of the magnetic field) is considered in the description of the electron drift with a proper treatment of the transverse and longitudinal diffusion effects, then the actual formation of the signal on the anodic strip is simulated, by taking into account the induction of the current, the presence of the resistive plane and the applied electronics. The digitization standalone code is borrowed from the code used in the BESIII CGEM-IT project to simulate the behavior of a triple-GEM: each step of the digitization is firstly studied by GARFIELD++ dedicated runs, from which the parameters are extracted and used to describe the physics effect under study in a simplified, fast, parametrized way. The effect of the resistive plate, which is present in the μ-RWELL but not in the GEM technology, was additionally studied and implemented. The charge density spread on the resistive layer has been described in [11] and [12]. The model has been adapted to a one-dimensional readout. The charge density spread depends on the charge produced in an avalanche, on its space and time distribution when entering the gap facing the anode and on the parameter called τ, i.e. the

This project has received funding from the European Union's Horizon 2020 research and innovation programme under grant agreement No. 871072.

decay time of the charge density due to the electrons movement towards the ground on the resistive surface. The effect of the APV-25 electronics is inserted in the simulation by its response function convoluted with the charge density spread.

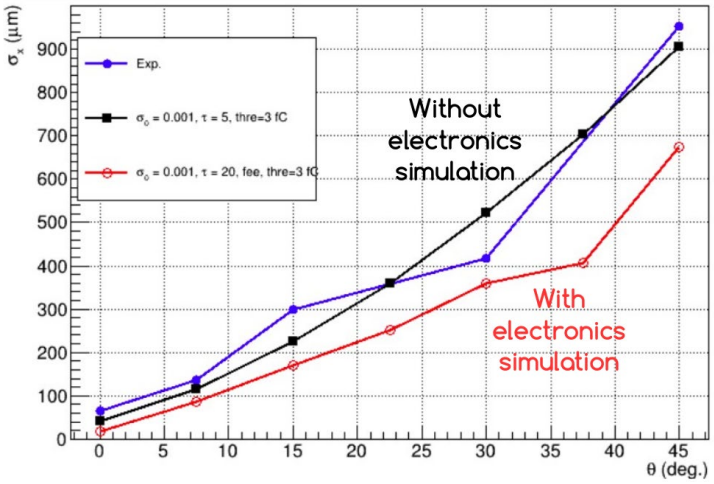

Figure 29. sigma of the charge spread distribution as a function of the track incident angle, simulated with (red) and without (black) the simulation of the electronics and extracted from experimental data (blue).

A preliminary evaluation of the sigma of the resulting distribution is shown in Figure 29, where the sigma of the position residual distribution as a function of the track incident angle is reported. The residual is computed as the difference of the position reconstructed via the charge centroid method and the MC point position. The black and red graphs are the simulation without and with the electronics simulation applied. Two different values of the τ time were used. The τ parameter will be the object of a fine tuning of the simulated data onto the experimental ones. Nevertheless, there is already a remarkable accordance between the simulated and real results.

A refined tuning procedure of the response simulation with experimental data is foreseen to properly reproduce the real detector performance. To this end, four sentinel variables have been identified that fully characterize the C-RWELL behavior: cluster size, cluster charge, position resolution obtained with the charge centroid and with the μTPC algorithms. The parameters of the simulation which need to be tuned are the τ time constant associated with the resistive plane and the threshold applied at readout time. Most probably also the gain value and the transverse/longitudinal diffusion will need a fine tuning, as well as the noise value, to have a satisfactory match of the simulated sentinel variables and the values extracted by the experimental data.

References

[1]. T.T Bohlen et al., The FLUKA Code: Developments and Challenges for High Energy and Medical Applications, Nuclear Data Sheets, 120, 211-214 (2014).

[2]. G. Battistoni et al., Overview of the FLUKA code, Annals of Nuclear Energy 82, 10-18(2015).

This project has received funding from the European Union's Horizon 2020 research and innovation programme under grant agreement No. 871072.

[3]. Frits A. Berends, P.H. Daverveldt, R. Kleiss, Monte Carlo Simulation of Two Photon Processes. 2. Complete Lowest Order Calculations for Four Lepton Production Processes in electron Positron Collisions, Comput.Phys.Commun. 40 (1986) 285-307
[4]. Frits A. Berends, P.H. Daverveldt, R. Kleiss, Complete Lowest Order Calculations for Four Lepton Final States in electron-Positron Collisions, Nucl.Phys. B253 (1985) 441-463.
[5]. S.Jadach et.al., in Physics at LEP2, edited by E.Altarelli, T.Sjostrand and F.Zwirner (CERN, Geneva, 1996), Vol.2, p.229, Yellow Report CERN 96-01, e-Print Archive: hep-ph/9602393.
[6]. G. Bencivenni et al., The micro-Resistive WELL detector: a compact spark-protected single amplification-stage MPGD, JINST 10 (2015) P02008.
[7]. G. Bencivenni et al., The μ-RWELL layouts for high particle rate, JINST 14 (2019) P05014.
[8]. A. Ochi et al., Carbon sputtering Technology for MPDG detectors, Proceeding of Science (TIPP2014) 351.
[9]. G. Bencivenni et al., On the space resolution of the μ-RWELL, JINST 16 (2020) P08036.
[10]. A. Amoroso et al., PARSIFAL: a toolkit for triple-GEM parametrized simulation, arXiv:2005.04452
[11]. M.S. Dixit et al., Position sensing from charge dispersion in micropattern gas detectors with a resistive anode, Nucl. Instrum. Meth. A 518 (2004) 721-727.
[12]. M. S. Dixit and A. Rankin, Simulating the charge dispersion phenomena in Micro Pattern Gas Detectors with a resistive anode, Nucl. Instrum. Meth. A 566 (2006) 281-285.

This project has received funding from the European Union's Horizon 2020 research and innovation programme under grant agreement No. 871072.